CHAPTER 2 LITERATURE REVIEW

2.1 Storage of natural gas in underground chambers

With the steady increase of the demand for city gas in urban area of many countries, its distribution capacity from liquid natural gas (LNG) plant in the coastal areas to consumers inland through existing pipelines is expected to reach its limitation in near future. To improve the reliability of gas service and upgrade the distribution facilities, it involves increase in pipeline length and storage capacity. The storage fulfills generally two basic requirements:

- provide system stability and higher efficiency in gas delivery (peak shaving)
- production of daily peak electric power with the aid of stored gas at night

To achieve these purposes also in long term, large agglomerations worldwide are planning to increase the present storage capacity of LNG. A Lined Rock Cavern (LRC) System with the concept of "Compressed Gas Energy Storage (CGES), which could contribute to more efficient management of the local and regional supplies of natural gas (Tengborg, 1989; Anderson, 1989), is proposed to enhance the efficiency of existing infrastructure and reduce additional investment. Although compressed gas has less density than LNG and therefore needs a greater geometric volume to store the same mass of gas, preliminary cost-benefit assessments indicated that CGES in large rock cavities would be more advantageous than LNG tanks on ground surface or buried just under the surface. Also the temperature can be kept over 0°C and environmental aspects favor the rock chamber solution owing to the very modest land use when compared to LNG tanks. The storage of Natural Gas in Underground Chambers includes 2 characteristics. It is the Lined Cavities at Shallow Depth and Unlined Cavities at deep depth. In this study will consider only the Lined Cavities at Shallow Depth.

2.2 Lined cavities at shallow depth

The most attractive feature of the lined concept resides in its low dependence on the hydrogeological conditions. The sealing against gas leakage is achieved entirely by an engineering barrier. A thin membrane assumes the task of permeabilization and the surrounding rock resists the enormous internal pressure. From this it follows that a high strength of the rock mass is still important but the permeability properties are of much less concern.

2.2.1 Depth determination

The depth of a lined rock cavity for CGES is determined on statical criteria. It is requested that the rock mass resists to the large gas pressure without unacceptable deformations or major fracture phenomena. Therefore, the main factors for depth determination are:

- Maximum gas pressure
- Initial state of stress in the rock
- Tensile strength of the rock mass
- Rock mass deformability.
- The depth could be determined according to a stress analysis upon the
- Criteria that the maximum existing tensile stress O-max must be less or equal to the tensile strength of the rock mass or, divided by a safety coefficient

$$\sigma_{max} < \sigma_t / F.$$

From these considerations it follows immediately that unavoidable uncertainty will arise from both the initial stress values and the rock mass tensile strength parameters. Both of these quantities are extremely difficult to measure or/and to assess with satisfactory reliability. Depth determination could also be considered from a purely safety point of view.

2.2.2 Rock mass strength

The strength of the rock mass plays a major role in two respects:

- Good quality rock requires little support or safety measures against break down
- High tensile strength of the mass limits propagation of cracks due to high internal gas pressure and permits, therefore, a shallow sitting of the scheme
- In case of unexpected gas leakage of the sealing high strength rock mass offers a major reduction of possible dramatic events
- Good quality/high strength rock mass - as a rule - has a low deformability. Therefore as will be analysed below - the strain which is imposed on the sealing membrane by deformation of the rock well will be smaller.

2.2.3 Lining concepts and lining materials

We define as lining the whole engineering structure which is installed on the rock surface for the purpose of rock support and gas impermeabilisation. From this follows that we can expect a type of sandwich structure. The function of rock support is well known. The function of impermeabilization for gas pressures of 70 to 100 or more is new. It is also important to realize the possible effects of outside ground water pressure in case of an empty cavity.

Criteria for selecting the sealing membrane:

- It must resist chemical corrosion of the stored product
- It must endure large local strain due to irregular deformations of the rock and due to open cracks of the underlying lining
- Consisting most probably of shotcrete
- It must exhibit little creep despite of the high requested strain (a particularly difficult clame to be fulfilled).

One of the most important requirements refers to leakage control. The chambers have to be tested by a 10% larger air or nitrogen pressure prior to being put into operation. If leakage is detected, its exact location must also be found. Gas leakage testing with the large individual cavity volumes is a difficult task.

2.2.4 Rock support of the cavity walls

The support of the rock wall is traditional. It will consist of rock anchors and shotcrete lining with steel mesh. As, however, the internal gas pressure will induce tensile strain into the shotcrete, this will inevitably be cracked. The task of a steel reinforcement in the shotcrete is to better distribute the cracks and fissures in order to limit the widening or closing of an individual gap. One of the most difficult problems still to be resolved concerns the prolongation of an existing rock joint into the shotcrete lining. If a rock joint opens and closes locally with a large aperture, this opening will also be imposed to the shotcrete by the shear-tight connection between shotcrete and rock. The steel mesh

in the shotcrete cannot prevent large cracks from developing. The only solution to this problem can be found by a sandwich construction allowing sliding of layers upon each other. In this way the sealing membranes can bridge major rock joints with wide opening. Puncture of sealing membrane must be avoided by all means. Rock support and lining should be safe against stress fatigue and creep of membranes. Fatigue of material can occur if the stress varies too frequently in a wide range.

2.2.5 Evaluation of the lined cavity concept

The lined cavity concept requires more engineering efforts for safe gas containment than the deep-seated unlined cavity concept.

Main advantages of the lined cavern concept:

- Shallow depth with short access, no requirements for long vertical shafts
- Access by spiral tunnels using conventional transport facilities for construction
- Clear sealing concept with clear engineering responsibilities. The sealing is an engineering product subjected to severe quality criterion.

Main disadvantages:

- The lining construction is still to be developed. Major research is to be initiated concerning chemical resistance against alteration and with respect to leakage proofing
- Maintenance of ground water drainage is to be granted during the whole operation life of the scheme
- Public acceptability is difficult to assess at the present stage of knowledge.

2.3 Consideration and configuration of lined rock cavern

The principal idea behind the LRC gas-storage concept is to rely on a rock mass (primary crystalline rock) to serve as a pressure chamber (Figure 2.1) in containing stored natural gas at maximum pressures from about 15 MPa to 25 MPa. The concept involves the use of relatively large, vertically cylindrical caverns 20 m to 50 m in diameter, 50 m to 115 m tall, with domed roofs and rounded inverts to maximize excavation stability. The caverns are located at depths from 100 m to 200 m below the ground surface, and they are lined with approximately 1-m thick reinforced concrete and thin (12-mm to 15-mm) carbon steel liners. (Figure 2.2)

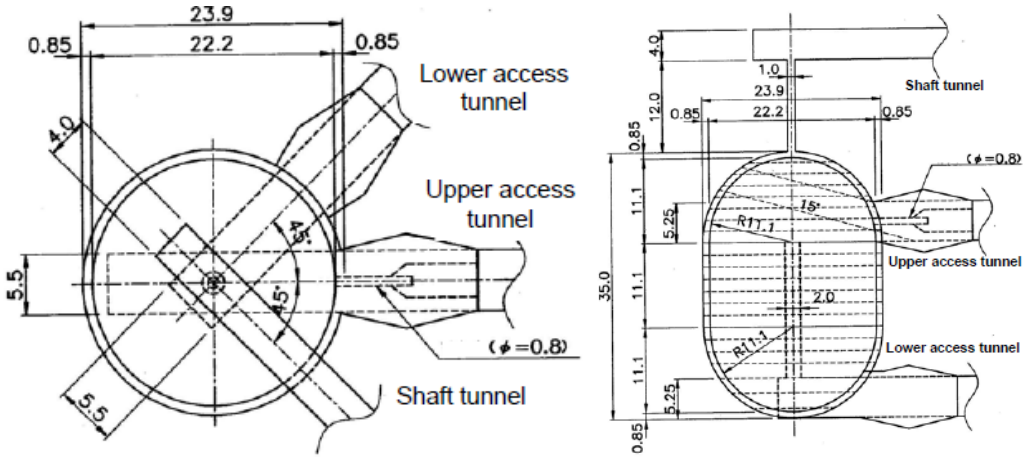

Figure 2.1 Schematic view of gas storage cavern (Larsson et al., 1989)

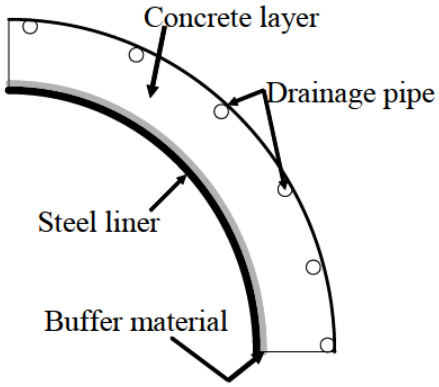

Figure 2.2 Lining materials (Tengborg ,1989)

The purpose of the steel liner, which is the innermost liner, is strictly to act as an impermeable barrier to the natural gas. The purpose of the concrete is to provide a uniform transfer of the gas pressure to the rock mass and to distribute any local strain in the rock mass (e.g., from the opening of natural rock fractures) at the concrete/rock interface more evenly across the concrete to the steel liner/concrete interface. To further minimize local circumferential strains in the steel liner, a viscous layer (about 5 mm thick) made of a bituminous material is placed between the steel and the concrete liners. Therefore, the methodology emphasizes two key LRC design criteria associated with (a) safety against ground uplift (Brandshaug et al., 2001), and (b) a maximum operating (cyclic) strain range in the steel liner (Branko, 2002). In this study, the discussion is concerned with the aforementioned first key aspect of the LRC concept: the ground uplift.

Pressurization of the gas increases the gas density (i.e., mass per unit volume) and is key to making the storage concept economically viable. An operating cavern is expected to go through pressure cycles from approximately 3 MPa to 25 MPa during periods of gas depletion and recharge, as demand dictates, and may have a nominal design life of 500 cycles. For circumstances in which groundwater is present, the gas pressure also provides structural support to the relatively thin steel liner, which is not designed to withstand external water pressure. It is expected that the LRC concept can be applied to a variety of different rock types and to rocks of varying strengths and deformabilities.

2.4 Assessment of uplift resistance

Two different limit equilibrium models, rigid-cone model and log-spiral model have been introduced in determining the safety and the depth of pressurized storage cavern to prevent from overburden rock mass failure (Brandshaug et al., 2001).

The rigid cone model assumes an overburden rock mass above caverns to be a cone shape. According to Littlejohn and Bruce (1975), the cone angle (α) is taken as 30° or 45°. Except for the cone angle, the model does not account for any rock mass strength, so that the rigid-cone concept is very simplistic relative to a real rock mass response.

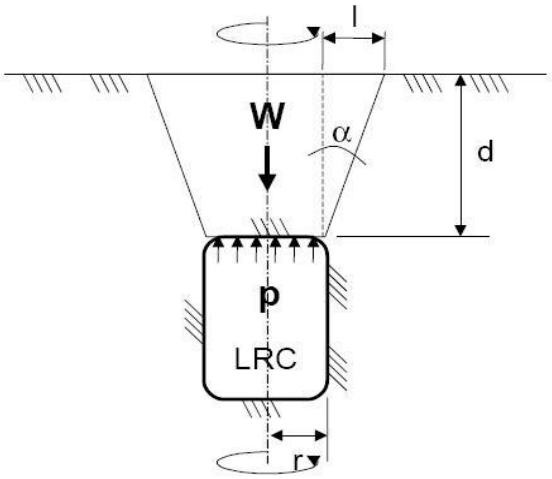

Figure 2.3 Rigid – Cone Limit – Equilibrium Model (Littlejohn and Bruce, 1975)

The log-spiral model is based on the response of soils in resisting a pull-out of soil anchor at shallow depth (Ghaly and Hanna, 1994). In addition to overburden rock mass weight, the model also includes the resistance from friction along the log-spiral failure surface. Mandl (1988) found the width and dip of the spirals to be sensitive to the amount of horizontal stress, and showed that the narrower and steeper dipping spirals were created with the lower horizontal stresses.

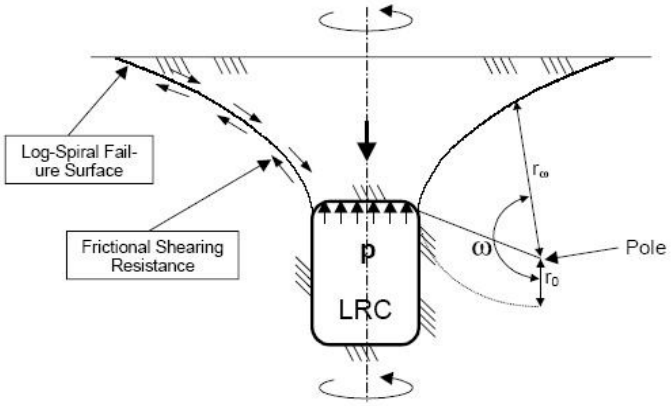

Figure 2.4 Log – Spiral Limit Equilibrium Model (Ghaly and Hanna, 1994)

A new model for ground uplift has been proposed to determine the safety and the depth of ground uplift above the silo-shaped pressurized storage cavern (Kim et al., 2012). The failure plane on the new model was assumed straight upward to ground surface (Figure 2.5) which has been considered in the previous Japanese research (Japan Gas Association, 2008). The straight failure plane model may produce more conservative and safer design criterions relative to the previous two models since the overburden weight determined by the straight failure plane geometry is smaller. But instead, the uncertainty regarding the angle of failure plane, of which information is difficult to be identified in advance, can be ignored. Buoyant force that is induced by groundwater

existence and is unfavorable in the safety against ground uplift was also included in theirs solution.

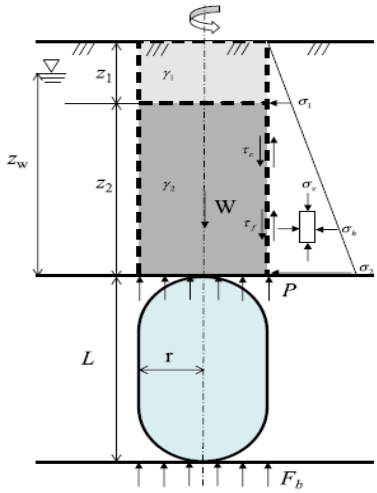

Figure 2.5 The straight failure plane model (Kim et al., 2012)

2.5 Fractures around underground cavities

To understand the way of fractures around underground cavities under high applied internal. Physical models and numerical model have been researched so that the discussions of this point refer to both of them.

2.5.1 Physical model test

The development of Fracture around cavities in rock is examined using physical. In uniaxial compression, the solution to the problem of fracture propagation is far from simple. Fracture around cavities is progressive. It may involve as many as three different processes: primary fracture at the tensile stress concentration, remote orsecondary fracture at positions inside the rock abutments (where a compressive maximum principal stress and a tensile minimum principal stress may combine to create critical conditions), and sidewall slabbing at the compressive stress concentration.

In recent years, (Dzik et al., 1996) investigated the evolution of fracture around a circular cavity loaded in uniaxial compression is at least qualitatively well established, the physical experiment was designed to provide quantitative data on the nucleation of the primary, the remote and the compressional fracture processes. For this purpose, a 200x200x60 mm. block of granite was cut and ground to accurate size .The 36 mm. holes was then drilled in the centre of the large face parallel to the least dimension. The instrumentation consisted of 19 strain gauges with a 5 mm long measuring grid that were bonded to be inside of the hole and to the surface of the block in positions where the primary, the remote, and the compressional fractures were expected to appear first (Figure 2.6). The actual locations were picked based on the experience gained in two earlier tests, using this granite in one and Beebe anorthosite in the other. In order to minimize friction at the rock-loading platen interface during the uniaxial compression test, two 30 mm.-thick granite loading platen were machined to match the size of the loading surface of the rock block. These were then inserted between the rock block and the loading platens of the testing machine. With the strain gauges connected to a data-acquistion system, the block was loaded in a 600,000 lb capacity testing machine to reach 157 MPa, producing an average ‘pillar stresses of 194 MPa. The mean uniaxial

compressive strength of intact Lac du Bonnet granite is 226 MPa. At the 157 load, all three element of fracture process were clearly displayed.

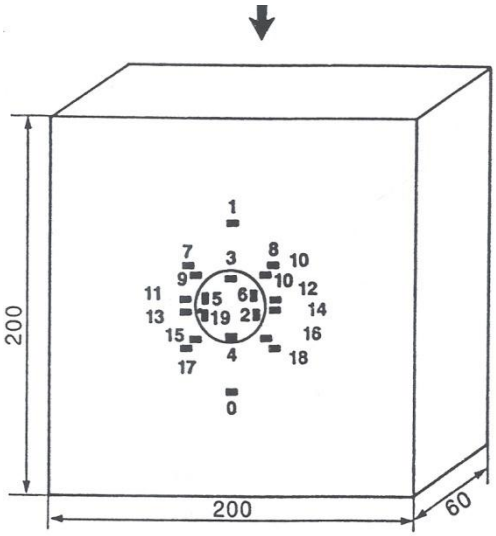

Figure 2.6 The granite test block with the strain gauge instrumentation. The gauge inside the hole were bonded to the inside wall. Loading was in uniaxial compression. (Carter et al., 1991)

Which the data collected on the relationship between axial stress and primary crack length at various cases of constant confining pressure are presented in Figure 2.7. The inserted trend lines, following the data suggest the expected stress-hardening; larger and larger stress increments are required to extend the crack as the cracks longer. The curves, shown for each confining pressure separately, are terminate where the remote fracture form.

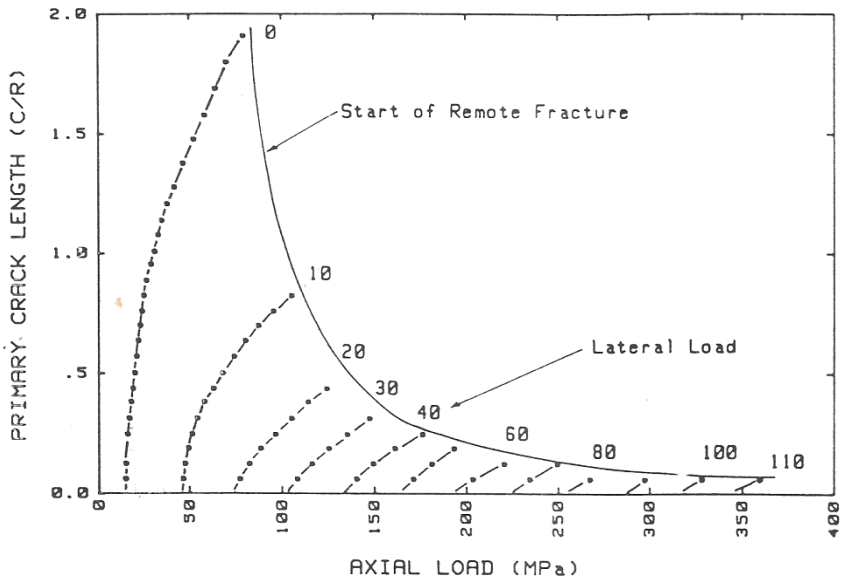

Figure 2.7 The primary crack length at the point of remote fracture nucleation for a range of confining pressure and as a function of axial load (Carter et al, 1991)

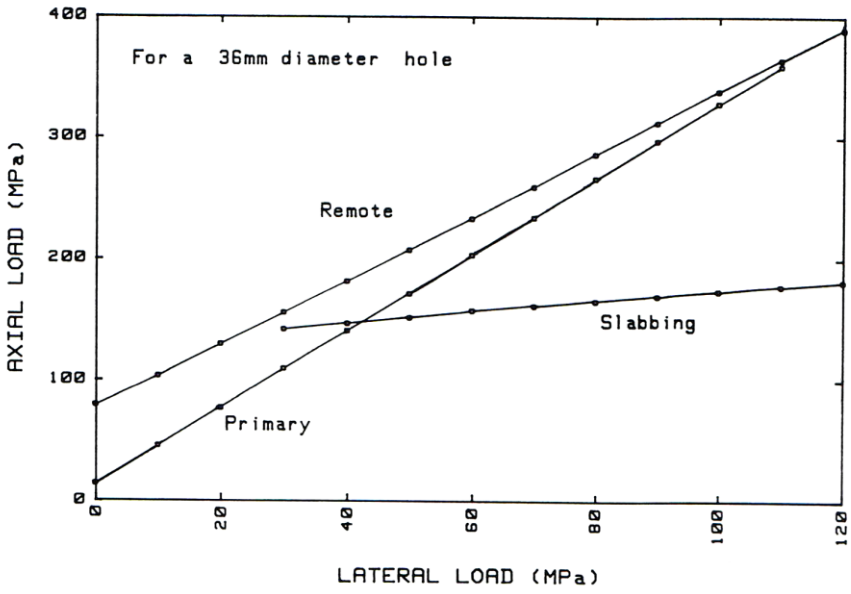

Figure 2.8 The critical for primary, remote and slabbing fracture. For each, the axial load increases linearly with the lateral load, although at different rate (Carter et al., 1991)

For all three types, the axial load at the point of fracture nucleation varies linearly with confining pressure (Figure 2.8). However, the rate of increase is different for each. The confining pressure seems to be the most effect in suppressing the primary fracture and the least effective in the prevention of the compressional failure.

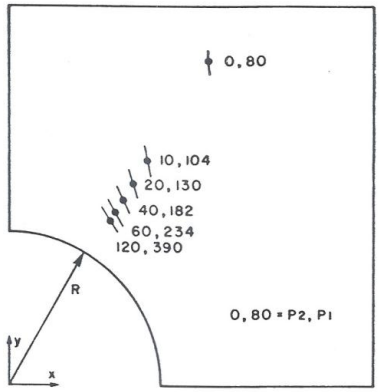

Figure 2.9 The locations of starting remote fracture change with confining pressure. As the confining pressure increases, the fracture moves closer to the perimeter and at the same time acquires a lower dip. The numbers identify the horizontal (P_2) and (P_1) loads (about 1/6 th of model is shown) (Carter et al., 1991)

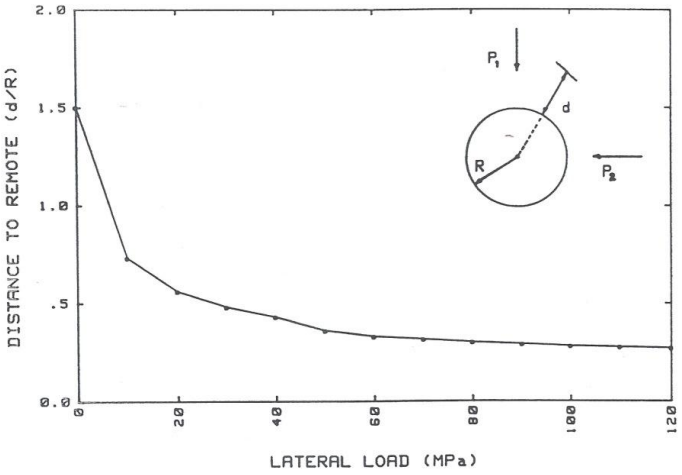

Figure 2.10 The distance to the point of remote fracture nucleation (Carter et al., 1991)

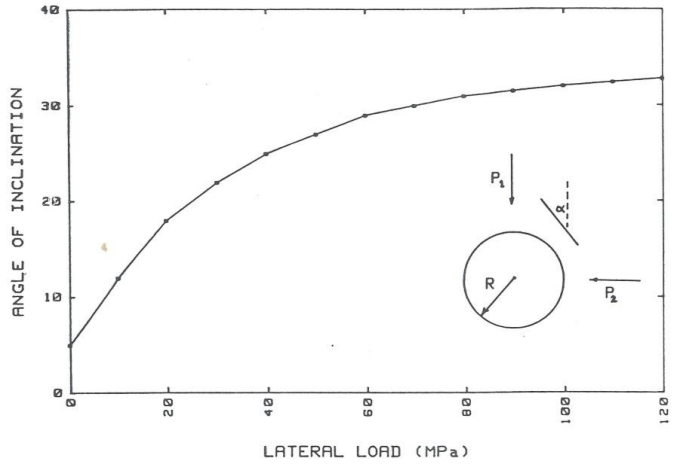

Figure 2.11 The inclination of the starting remote fracture changes from almost vertical at uniaxial load to just above 30º at high confining pressure (Carter et al., 1991)

The location of starting remote fracture changes with confining pressure (Figure2.9). On increasing confining pressure, the point of nucleation move closer to the opening (Figure 2.10) and at the same time acquires a shallower dip (Figure 2.11).The starting remote fracture is practically vertical at no confining pressure, but would rotate to a dip of about 60° at high confining pressure.

Dzik and Lajtai (1996) studied the evolution of fracture around cavity, which will test blocks were machined from Lac du Bonnet granite purchased from the Cold Spring Quarry located near Lac du Bonnet, Manitoba. This rock is unfractured so that making blocksas large as 750 x 500 x 100mm created no problem. Each block had a central cylindrical cavity drilled out along the minimum dimension. The block sizes were varied so that the width of the block (intermediate dimension) was at least 10 times the radius of the central cavity (R).The granite is a medium grained, strong, brittle, elastic rock with elastic modulus of 70 GPa, Poisson's ratio of 0.2, uniaxial compressive strength of 226 MPa, Brazilian tensile strength of 14 MPa and fracture toughness of 2.45 MPax/m. Each block was instrumented with as many as 40 strain gauges, placed strategically to detect and follow the fractures in the primary, remote, and slabbing

positions (Figure 2.12). The uniaxial compressive load was applied with a 5000kN capacity MTS testing machine in stress-control mode. However, the loading rate was varied to allow periodic visual examination of the fractures. In general, a test would take between four to six hours to complete. During this time, the compressive stress on the rock blocks was increased to about 150 MPa. The stress level was usually sufficient to generate all three fracture processes without causing the collapse of the cavity. Boundary conditions have always posed difficulties in laboratory testing. For this work the granite blocks were tested with several types of boundary conditions. A typical test had steel platens directly in contact with the granite block. Noteworthy is a set of crack propagation tests performed on three identically sized blocks containing/~ = 40 mm holes. The first case had a teflon insert placed between the steel platen and the sample. The second case was with the steel platen only and the third case had a granite platen glued directly to the sample with a steel platen placed on top. At a steel-granite interface a substantial amount of friction usually develops resulting in greater stability of the sample. This was not the case here. In all three tests the primary fractures propagated through the samples at similar stress levels in almost unstable fashion. In light of these findings it was assumed that boundary influences were limited and the effects shown by the crack propagation results could indeed be attributed to a size effect.

Figure 2.12 Testing of a large granite block (R = 50 mm) (Dzik and Lajtai, 1996)

Tunsakul et al. (2013) studied the investigation of failure behaviors of rock mass surrounding the underground cavern under high internal pressure through a series of physical model tests under 1-g scaled-models. Using this approach, the experimental sample size is decreased by 200 times (Figure 2.13) of the prototype which is designed as a silo-shaped underground cavern. The physical model is then a silo of 0.1 m in diameter and 0.2 m high. The depth of the cavern center in the model is 0.5 m (under the ground surface). The rocks are simulated from mixtures of plaster, sand and water. In order to investigate the failure behavior, only a quarter of the entire problem is considered. Six tests including 2 vertical in-situ stresses (representing the depths of 125 and 250 m) and 3 lateral earth pressure ratio (K_o = 0.5, 1 and 3) are conducted. During the tests, the internal pressure is progressively increased until a crack is initiated and progressive failure is shown (Figure 2.14 and 2.15). The strain field from photogrammetric analysis is used to capture behavior of rock mass around the cavern. The location of predominant crack is observed as well. The results reveal that the lateral earth pressure coefficient at rest, K_o has a strong influence on the position of the crack initiation point. Under condition of K_o less than 1, the failure path that initiated from cavern edge tends to move upward to the ground surface.

Figure 2.13 Tested specimen decreased by 200 times 0.50x0.50x0.95 m3 (Tunsakul et al., 2013)

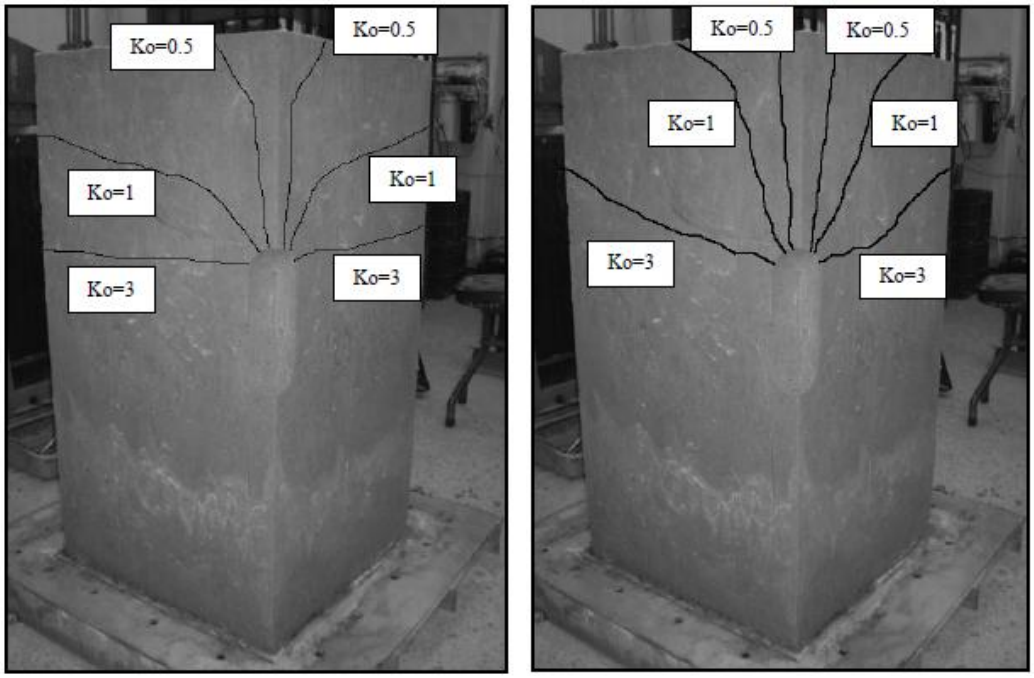

a) Deep equivalent vertical stress 125 m b) Deep equivalent vertical stress 250 m

Figure 2.14 All failure paths after testing condition under all initial K_O (Tunsakul et al., 2013)

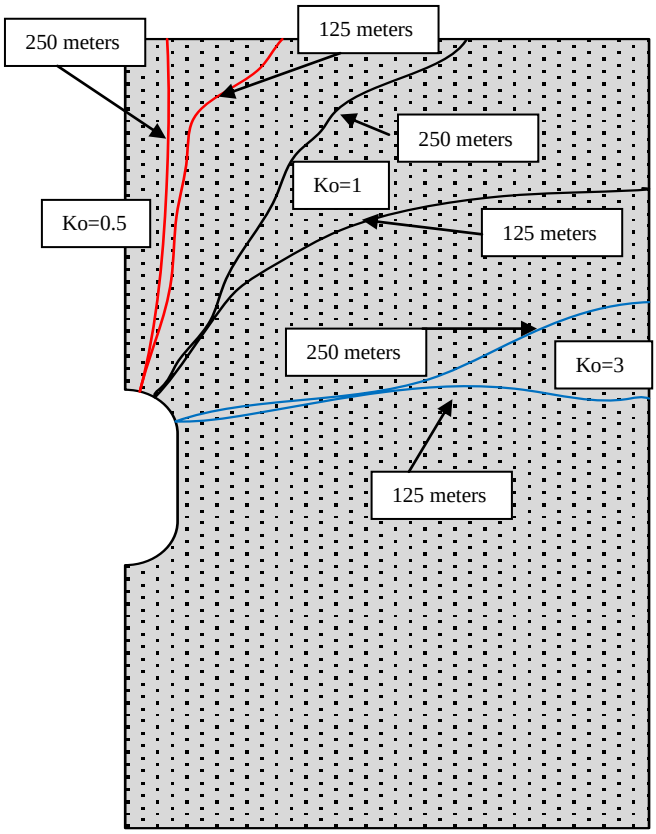

Figure 2.15 All failure paths from all initial vertical stresses after testing condition under all initial K_O (Tunsakul et al., 2013)

1. Fracture nucleation

The formation of the first fracture was deduced from the output of strain gauges placed in the nucleation positions. For primary fracture and slabbing, the fracture started at the perimeter of the cavity. For the larger radii cavities (R > 20 mm), it was possible to attach a strain gauge to the interior curved face of the cavity (Figure 2.16). For the smaller cavities, the point of nucleation was interpreted from the first gauge fixed on the face of the block, just above the perimeter (Figure 2.17). Strain gauge G1 in Figure 2.11 is placed directly on the greatest tensile stress concentration created by the circular opening. Because of this, the Young's modulus calculated from the response of this gauge does not reflect the bulk properties of the rock mass as do the gauges further from the opening. As expected the fracture nucleation stress, for all three fracture types, was size-dependent with size sensitivity being the most prominent in the small radius range (R < 10mm) (Figure 2.18).

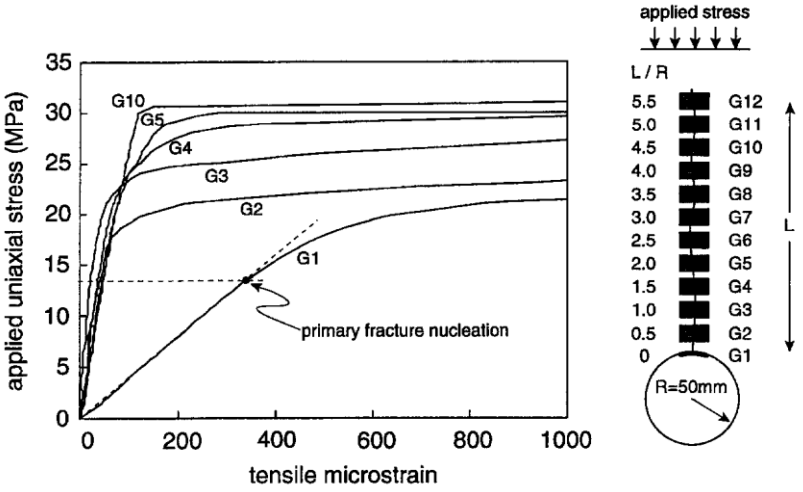

Figure 2.16 Typical strain gauge response to uniaxial loading of an R = 50 mm sample. Dzik and Lajtai, 1996)

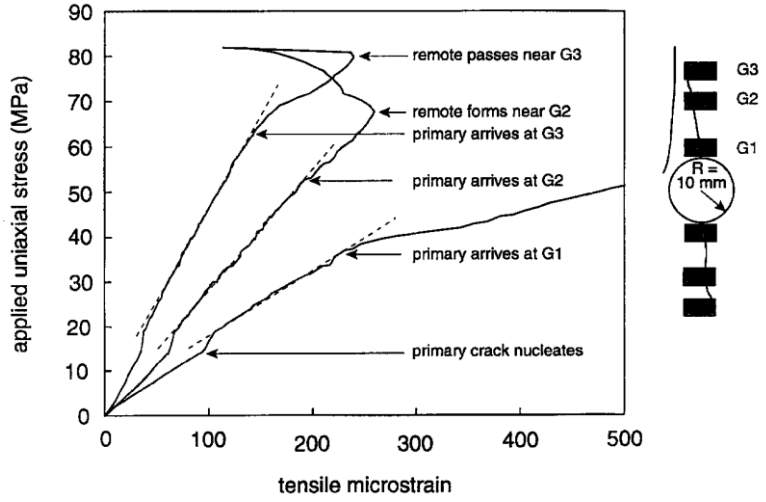

Figure 2.17 Typical strain gauge response to uniaxial loading of an R = 10 mm sample. (Dzik and Lajtai, 1996)

2. Fracture propagation

Following nucleation, the extension of the primary fracture in response to increasing uniaxial load was followed visually and through examination of the response of the strain gauges fixed along the fracture path. Interpreting the output of the strain gauges involves some judgment in pinpointing the crack-tip location. Figure 2.11 and 2.12 illustrate this procedure. For the large cavities, the internal strain gauge would always clearly indicate the point of nucleation at the yield point of the strain curve (Figure 2.16). Lac du Bonnet granite is truly a linear material, so the deflection of the curve could only be the result of fracture nucleation. For the external gauges, the interpretation is somewhat more difficult. In general, all strain gauges in the vicinity of the nucleation point would show some signs of disturbance. For the 10 mm cavity of Fig ure2.12, all three gauges show momentary strain relief on nucleation. The arrival of the crack tip is signalled by the deflection of the load-strain curves after a period of continuing elastic deformation following the initial strain relief. Visual examination of the 10 mm sample showed that the crack tip barely reached the gauge 3 position.

However, the response from the large radius holes was quite different. After an initial phase of stable crack growth (gauges 1 to 5), the propagation rate accelerated with the crack tip running through gauges 6 to 10 with only a slight increase in load (strain gauge curves left out of Figure 2.11 for clarity). Cavities of intermediate radii showed transitional behavior (Figure 2.19).

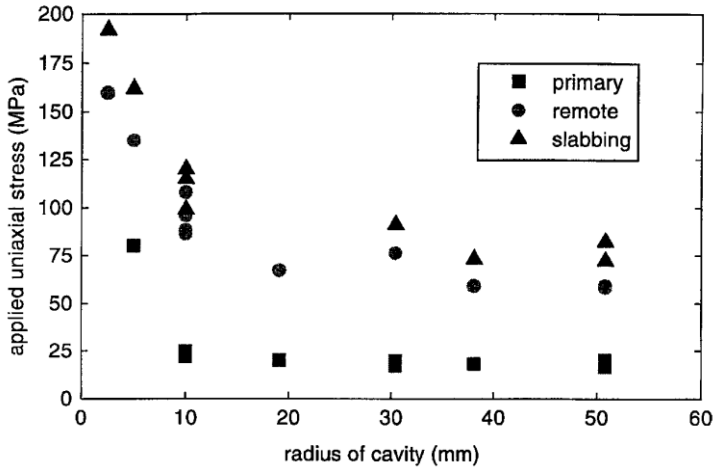

Figure 2.18 Crack initiation data collected from laboratory testing. (Dzik and Lajtai,1996)

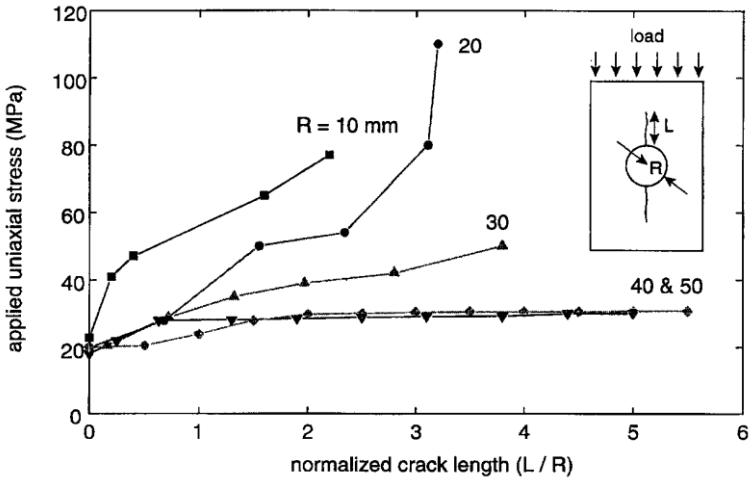

Figure 2.19 Crack propagation data collected from laboratory testing. (Dzik and Lajtai,1996)

Three types of fractures are associated with cylindrical cavities loaded in compression: primary fractures nucleating at the tensile stress concentration of the perimeter, remote fractures at points remote to the perimeter where a combination of tensile and compressive stresses create favorable conditions for fracture, and slabbing fractures that form at the compressive stress concentrations of the perimeter. Not all the fracture types need to form. Their formation depends on loading conditions and the size of the cavity. The propagation of primary fractures nucleating at the tensile stress concentration of the perimeter of a cylindrical cavity (tunnel) is size dependent. The overall trend of crack extension suggests very stable crack growth for small cavities ($R < 20$ mm) and tending to almost unstable crack growth for large cavities ($R > 40$ mm). Cavities of intermediate

size display transitional behavior. For small cavities the propagation of the primary fracture is arrested when remote fractures appear. In the loading of very small cavities (R < 3 mm) there are no primary fractures. Only remote fractures appear.

2.5.2 Numerical model test

In more recent developments, micromechanical models have been developed to simulate the instability or loss of integrity of a tunnel or borehole. These models have improved the understanding of the mechanisms and consequences of fracture initiation and propagation. For example, the non-linear rule-based model (Blair and Cook, 1998), the lattice model (Chinaia et al., 1997) and the bonded particle model et (Potyondy et al., 1996; Hazzard and Young, 2000) have been found to be capable of simulating the fracture process of quasi-brittle materials such as rock by accounting for microscopic aspects of rock fracture and the crack propagation mechanism (Germanovich and Dyskin, 2000). These models could be used with more confidence to examine in detail the nature of damage and failure in rocks. However, none of these reported models are capable of simulating the progressive fracturing process in rocks around underground openings, which is characterized by initiation, propagation and coalescence of cracks, resulting in strain localization and stress redistribution.

In the current study, RFPA (Rock Failure Process Analysis), a well-recognized numerical code, has been used to simulate the progressive fracturing processes in rocks around underground openings. The investigation has been conducted for common cross-sectional shapes of underground openings, including circular, elliptical and inverted U-shapes, under different loading conditions. RFPA has been used extensively to simulate the failure process of rocks in a number of engineering fields (Tang, 1997; Tang and Hudson, 2002; Tang and Kaiser, 1998; Zhu and Tang, 2002, 2004). The unique feature of this code is that no a priori assumptions need to be made about where and how fracture and failure will occur cracking can occur spontaneously and can exhibit a variety of mechanisms when certain local stress conditions are exceeded. In the investigation, because the shape of an opening may change when the fracture zone around it initiates and grows, the numerical simulation has been formulated to take account of this change during the failure process. In addition, the influence of the failure zone on the stress distribution in the remote compression zone is considered in order to study the evolution of fractures around the underground opening.

1. Models of underground openings

In the following simulations, three simple shapes of underground openings, with circular, elliptical and inverted U cross-sections, are considered. The specific geometries and loading conditions for these three geometries are shown in Figure 2.20. Applied boundary stresses in the vertical and horizontal directions are denoted as p and kp, respectively, where j is usually called lateral pressure coefficient. These models have a common dimension of 240 mm 240 mm. The diameter of the circular opening, the transverse axis of the elliptical opening and the width of the inverted U-shaped opening are all 1/4 of the length of the whole model. These cases of simple excavation geometries and an assumed homogeneous rock mass with known elastic properties are examined as reference or base cases for the subsequent analyses with RFPA^{2D}, which take account of heterogeneity of the medium and damage associated with fracture formation.

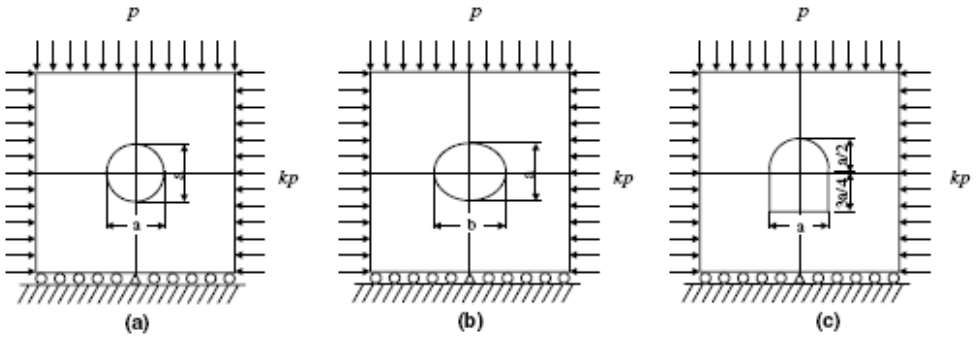

Figure 2.20 Geometries and loading conditions for openings with circular, elliptical and inverted U-shaped cross-section. p and kp are pressures applied in vertical and horizontal direction of specimens, j is the lateral pressure coefficient. (Zhu et al., 2005)

2. Boundary stresses around excavations

In order to understand the failure mechanism of the host rock for the model excavations, the stress distribution is solved first. When the state of stress in rock around the opening is calculated based on the theory of elasticity, for the circular and elliptical openings subjected to uniaxial or biaxial stress states, the stress distributions in the host rock are provided by well- known analytical solutions. For the inverted U-shaped opening, the stress distribution is obtained though finite element analysis.

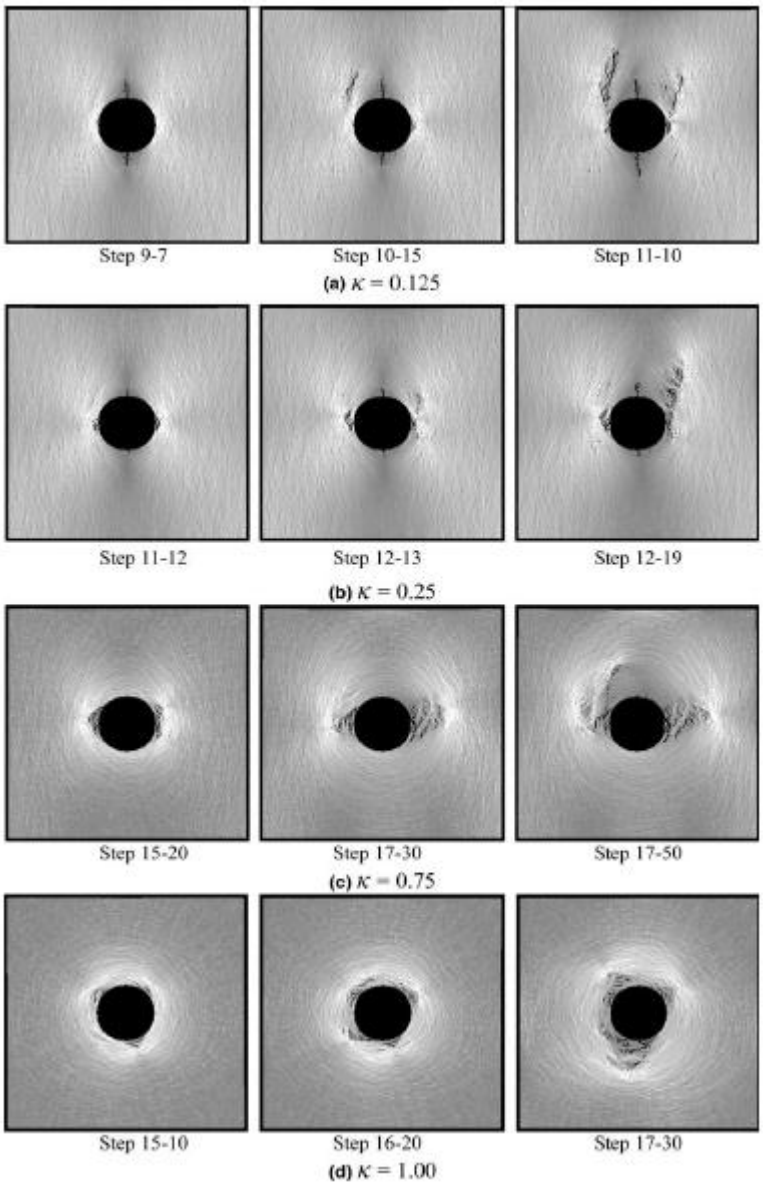

Figure 2.21 Failure patterns of rock around circular openings for different lateral pressure coefficients. The applied pressure in the vertical direction is fixed at 4 MPa/step. For each lateral pressure coefficient, the maximum shear stress distributions at three typical steps are given. (Zhu et al., 2005)

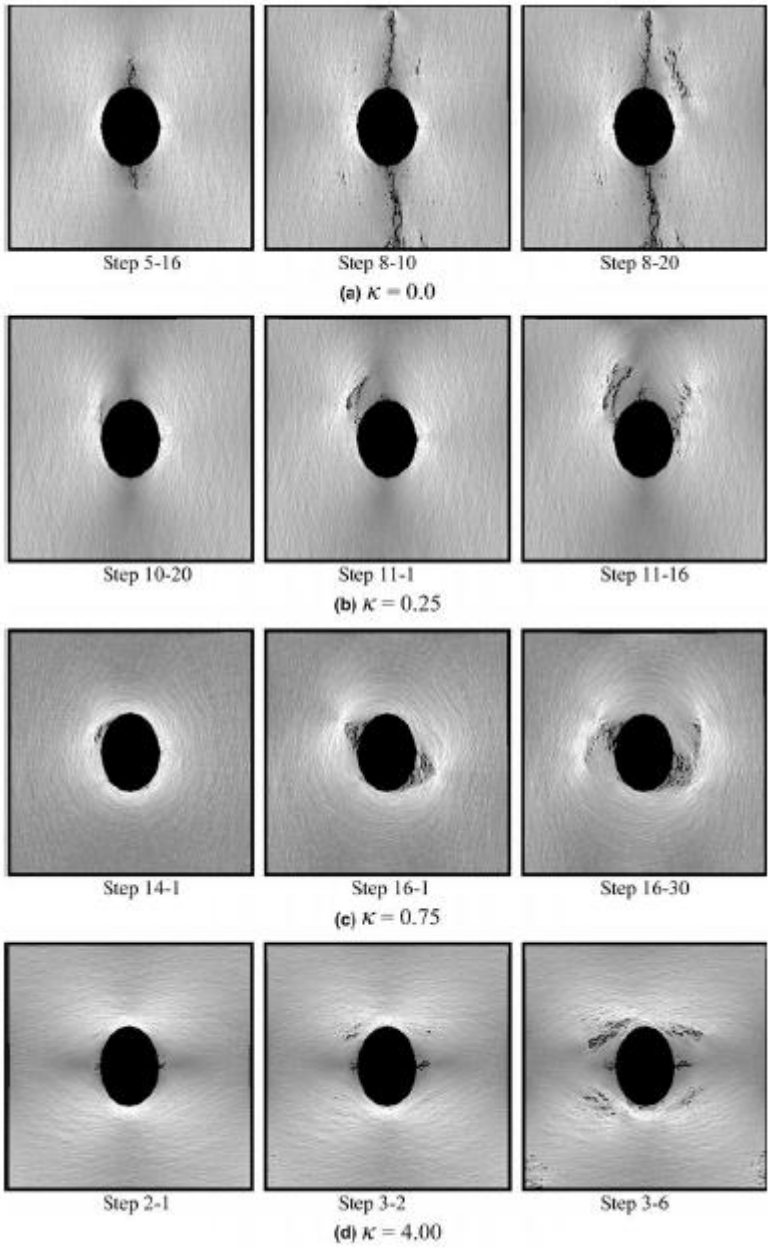

Figure 2.22 Failure patterns of rock around elliptical openings for different lateral pressure coefficients. The applied pressure in the vertical direction is fixed at 4 MPa/step. For each lateral pressure coefficient, the maximum shear stress distributions at three typical steps are given. (Zhu et al., 2005)

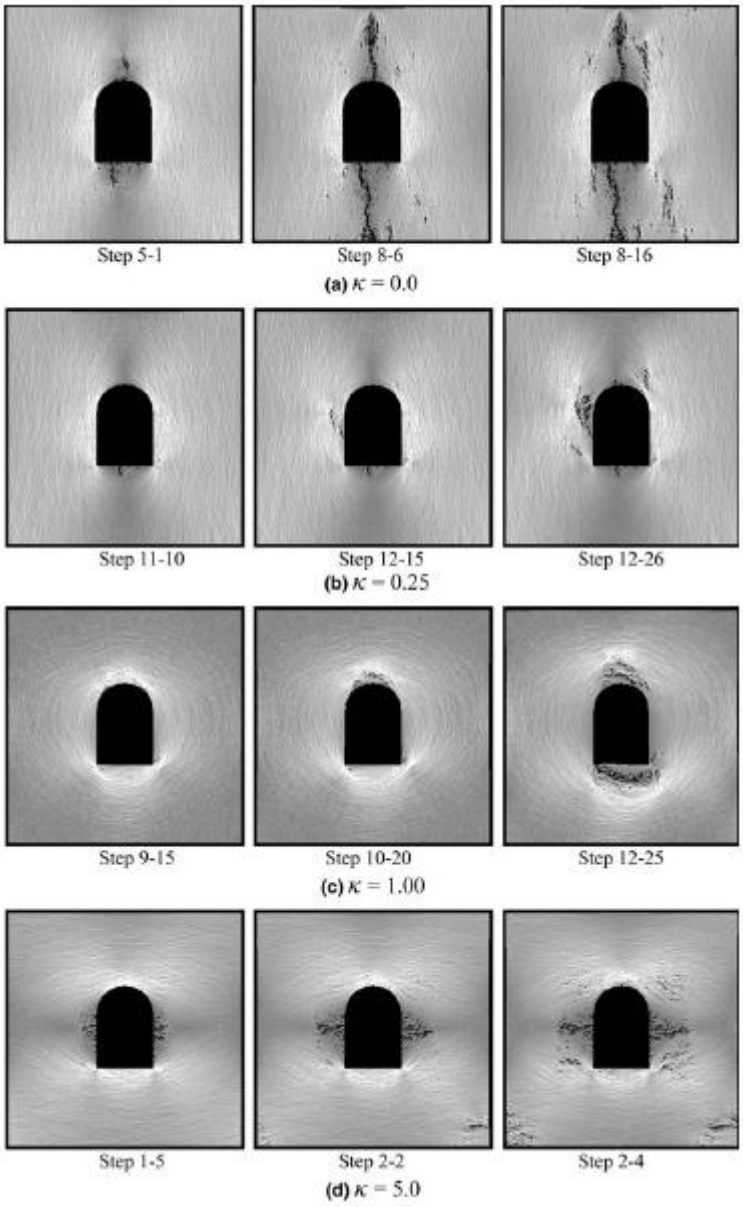

Figure 2.23 Failure patterns of rock around inverted U-shaped openings for different lateral pressure coefficients. The applied pressure in the vertical direction is fixed at 4 MPa/step. For each lateral pressure coefficient, the maximum shear stress distributions at three typical steps are given. (Zhu et al., 2005)

The numerical code RFPA has been applied to simulate the failure process and the path to collapse of different shapes of underground openings under uniaxial or biaxial loading conditions. Based on the results from the simulations, the following conclusions are described.

For a circular opening under uniaxial compression or a low lateral pressure coefficient, a primary tensile crack, a remote tensile crack and a shear crack develop. For lateral pressure coefficients are less than 0.25, the applied stresses required to form the primary tensile crack and for excavation collapse increase with increasing lateral pressure. When the lateral pressure coefficient is 0.75 or 1.0, no primary tensile cracks develop, and the

state of stress at the initiation of shear damage increases with the lateral pressure. For an elliptical opening, remote cracks, accompanied by the primary tensile crack, are formed when the lateral pressure coefficient is much smaller or much larger than the ellipse shape factor a/b, where a and b are the ellipse semi-axes. The remote cracks are caused mainly by tensile damage as the first primary tensile crack increases in length. For an inverted U-shaped opening, a remote crack is observed when the confining pressure is relatively low. For the hydrostatic case (k = 1.0), shear fractures develop in the roof and floor of the opening, and no remote crack is formed. For k = 4.0, primary tensile cracks are formed in the sidewalls, and remote cracks, caused by the tensile damage, are also formed.

2.5.3 Numerical and experimental investigations on fractures in gas storage cavern

A series of physical and numerical model tests were performed to investigate the failure behaviors of continuous rock mass surrounding the silo-shaped cavern under high internal pressure by Tunsakul et al. (2013). Theirs research aims at providing the information on fracture initiation and propagation in rock mass around underground gas storage cavern occurred from applying high internal pressure under different controlled conditions. By scaling down the prototype 200 times (Figure 2.13), synthesis rock specimens containing silo-shaped hole were confined to vertical pressures of 12.5 and 25 kPa with confinement regarding to Ko of 0.5, 1 and 3 in the two horizontal directions. The pressure was gradually applied in the silo until the fracture is initiated and propagates. The photogrammetric analysis provides insights into the response of rock mass during the application of the internal pressure and assists in identifying the occurred failure path. The resulting fracture patterns indicated that the lateral earth pressure coefficient at rest, Ko, has strong influence on the position of crack initiation and the propagation direction of failure path. Supplemental numerical analyses were carried out to investigate the failure mode which cannot be covered by the model tests. The numerical 3 method on the basis of FEM considering stress analysis with the localization is developed to capture the formation of discrete fracture in a continuum. It is found that the method is able to represent the factors that affect the fracture pattern and the qualitative agreement between the experimental and numerical results can be established. The comparison between experimental and numerical results leads to the conclusion that the fracturing process was caused by tensile cracking (Figure 2.24).

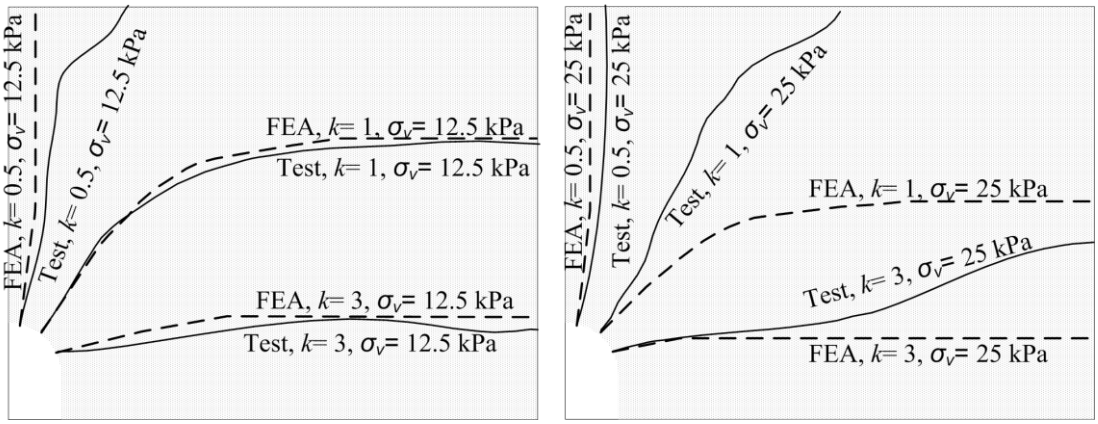

Figure 2.24 The comparisons of failure paths obtained between numerical analyses and physical model tests (Tunsakul et al., 2013)

2.6 Progressive failure analysis of high-pressure gas storage cavern

2.6.1 Localization and progressive failure

1. Progressive failure

In reality, shear strain is distributed. At certain stage, it is localized and formed a failure plane. To analyze localization problem, it requires very heavy computations in FEM. It has been known that the results of the analysis in which distributed failure surfaces are localized into one failure surface, are not so different from that of the analysis in which one failure surface is assumed from the beginning. Then, a simplified analysis method was adopted in this study. That is, a path of failure surface in rock mass is assumed in advance based on stress filed obtained from the preliminary analysis. Along this predicted path, shear sliding starts when the failure condition is satisfied in the analysis.

2. Interface interaction model

A special attention is paid to the interface of rock mass along failure path as displacement discontinuity, namely sliding, under certain stress conditions. The interfaces between rock masses follow an elastic-plastic stress-displacement relation. The condition for a relative slip along an interface is governed by a Coulomb law. If the tensile strength of the contact, which is usually zero, is overcome, the surface separate, creating a gap between them. The finite element program used in this study, ABAQUS, provides an interface contact element which is possible to model both normal and friction behaviors separately. The schematic element of interface is illustrated in Figure 2.25.

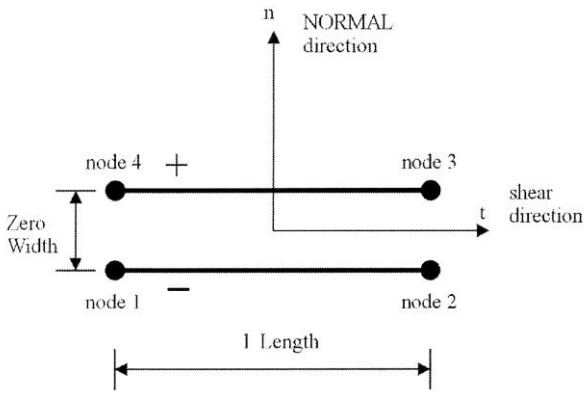

Figure 2.25 The interface contact element (Jongpradist et al., 2007)

For the behaviors in normal direction, in this study, it is treated to be opened under tension. The closed condition is assumed for pre-slip behavior and no penetration for post-slip under compression. Whereas, the friction behavior in shear direction for pre-slip is assumed to be sticking condition and perfectly smooth for tension. The post-slip behavior of friction behavior is assumed to follow Coulomb law and the cohesion becomes zero.

2.6.2 Basic algorithms for analysis

1. Preliminary analysis

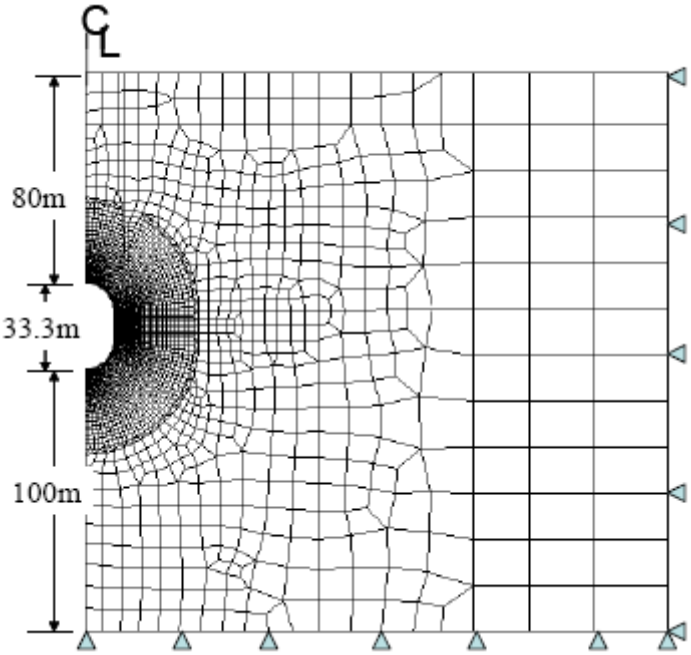

Figure 2.26 Axis-symmetry analytical meshes (Jongpradist et al., 2007)

Firstly, an analysis of cavern under the inner pressure of 15.6 MPa (1.3 time of maximum operation pressure, 12 MPa) using a FEM program is carried out in order to obtain the stress field. The cavern with an inner diameter of 22.2 m and 33.3 m tall is located in rock at a depth of about 100 m. The geometry, boundary condition and FE mesh used for the analyses are shown in Figure 2.26. Axis-symmetry state is assumed. The geological material is divided into 3 parts which are rock mass, top soil (uppermost 20 m) and excavation disturbed zone, EDZ (1 m thick around excavation surface). Material parameters used in the analysis are listed in Table 2.1 and 2.2

Table 2.1 Properties of rock masses (Jongpradist et al., 2007)

	Unit weight,γ (kg/m^3)	Young's modulus (GN/m^2)	ν	$\phi(^\circ)$	C (MN/m^2)
Rock mass	2,600	6.66	0.3	45	3.0
EDZ	2,600	2.66	0.4	38	1.3
Top soil	2,000	1.0	0.4	30	0.5

Table 2.2 Material parameters of concrete liner (Jongpradist et al., 2007)

E (GN/m^2)	Compressive strength (MN/m^2)	Tensile strength (MN/m^2)	ν
28	30	2.2	0.2

The results of analysis are shown in Figure 2.27 and 2.28. Figure2.27 illustrates the distribution of the computed Local safety factor, *Lsf*, which is defined as,

$$\text{Lsf} = \frac{\tau_s}{\tau} = \frac{2C\cos\phi + (\sigma_1 + \sigma_3)\sin\phi}{\sigma_1 - \sigma_3} \quad (2.1)$$

where C and φ are cohesion and friction angle of each geomaterial. The parameters σ1 and σ3 stand for maximum and minimum principal stresses, respectively. It is found that the minimum Lsf of 1.07 is at the rock mass adjacent to the concrete liner on the roof of cavern with the angle of 45 degree from the center line.

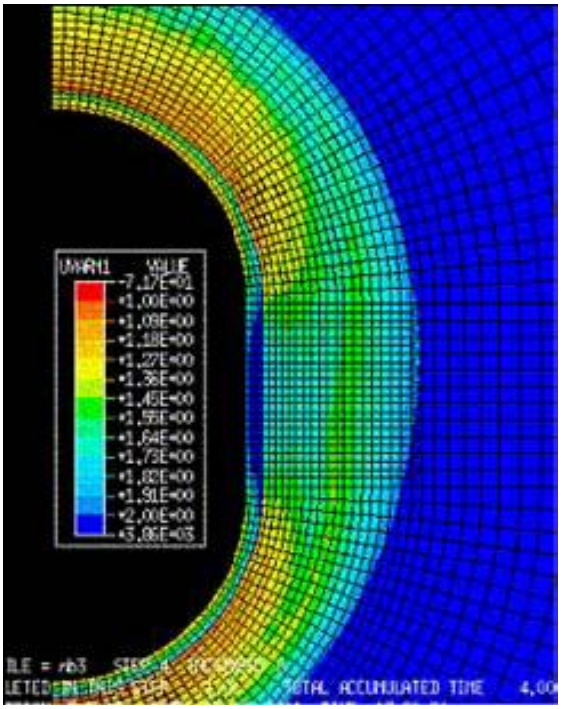

Figure 2.27 Distribution of local safety of factor at the inner pressure of 15.6 MPa (Jongpradist et al., 2007)

Figure 2.29 depicts the orientation of failure plane computed from stress state using equation (2). By connecting the direction vectors starting from the point with minimum Lsf, the failure surface is obtained.

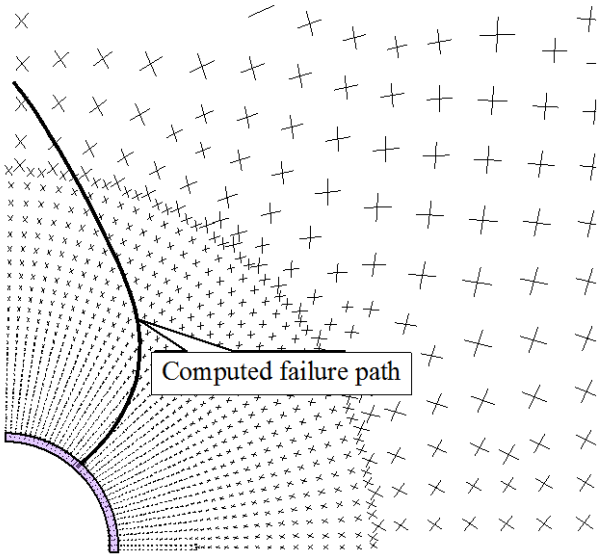

Figure 2.28 Computed failure path from stress state of preliminary analysis (Jongpradist et al., 2007)

2. Prediction of failure path

In this section a method to predict the failure path which will be used in progressive failure analysis in the next section is presented. First the stress state at the inner pressure of 15.6 MPa is obtained from preliminary analysis presented in the previous section. The principal stress direction and accordingly the orientation of failure plane at any location, θ_0, are calculated as:

$$\theta_0 = \frac{1}{2}\cos^{-1}\frac{(\sigma_1 - \sigma_3)\tan\phi}{2C_r - (\sigma_1 + \sigma_3)\tan\phi} \tag{2.2}$$

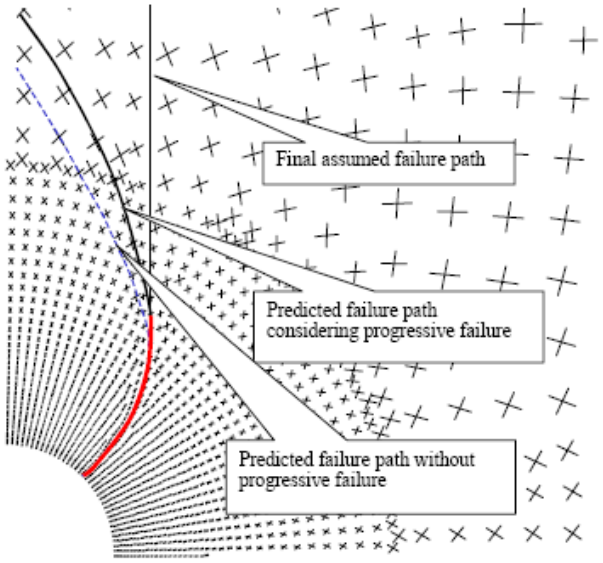

Figure 2.29 Computed failure surfaces with and without considering progressive failure (Jongpradist et al., 2007)

The point along cavern surface which has the minimum local safety factor (Lsf) is selected as the starting point for failure path. By connecting the direction of failure plane at any locations, the failure surface is obtained. It should be noted that the predicted failure path obtained from this procedure might not be correct since it is based on a certain stress state obtained from preliminary analysis without failure and associated stress redistribution. Thus, to obtain more accuracy, analyses of underground cavern under inner pressure considering partial failure were carried out and the stress redistribution was evaluated for orientation of failure plane. The results indicate the change of failure surface moving upward to the ground surface as shown in Figure 2.29. The final predicted failure path is then estimated to be as shown in Figure 2.30.

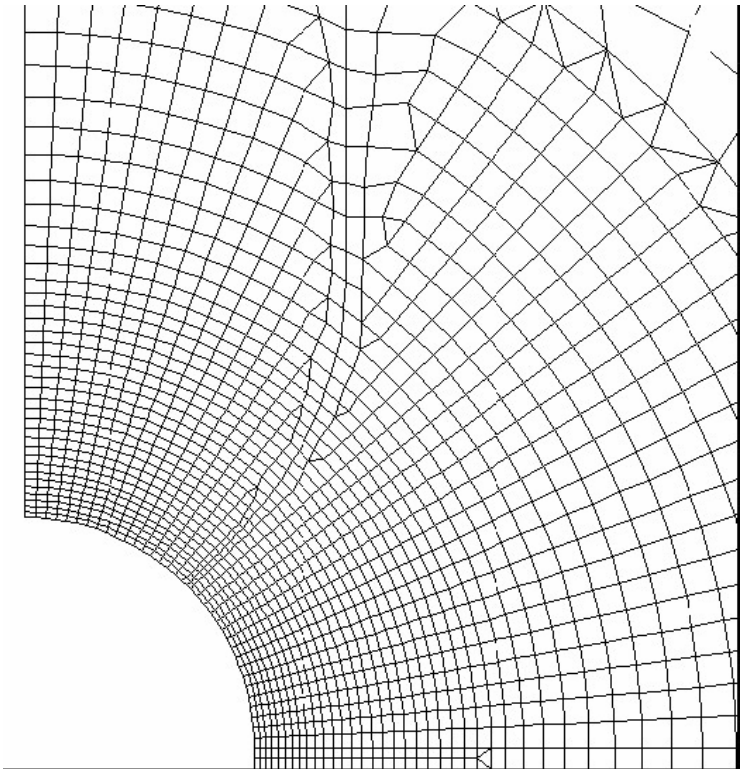

Figure 2.30 Final analytical mesh including failure surface (Jongpradist et al., 2007)

3. Interface Failure Criterion

In this study, it is assumed that the failure occurs when the shear stress along the predicted failure surface exceeds the Mohr- Coulomb shear strength as written in equation 3.

$$\tau > C + \sigma_n \times \tan\phi \tag{2.3}$$

Once the stress state attains the failure criterion, slip starts and the cohesion becomes zero. The post-failure behavior of interface is then assumed to follow Coulomb law as;

$$\sigma_s > \sigma_n \times \tan\phi \tag{2.4}$$

4. Uplift analysis considering progressive failure

Table 2.3 Analysis cases by varying shear strength parameters (Jongpradist et al., 2007)

Case		Shear strength parameters		Post failure
		C'(Mn/m^2)	ϕ(°)	
1	Rock mass	3.0	45	Post failure :$C=0$
C'=C	Top soil	0.5	30	
2	Rock mass	0.9	45	Post failure :$C=0$
C'=0.3C	Top soil	0.15	30	
3	Rock mass	0	45	
C'=0	Top soil	0	30	

The analysis of cavern stability against inner pressure using the final analytical mesh is then carried out. The analytical mesh was modified to include the predicted failure surface and the interface contact elements were embedded along that failure surface. In the analysis, the inner pressure increases step by step up to 26 MPa (2 times of operation pressure) and the stress state along the predicted failure surface is evaluated.

2.6.3 The effect of gas storage cavern on failure length

The failure length (Lf) during applying the inner pressure is observed as shown in Figure 2.31.

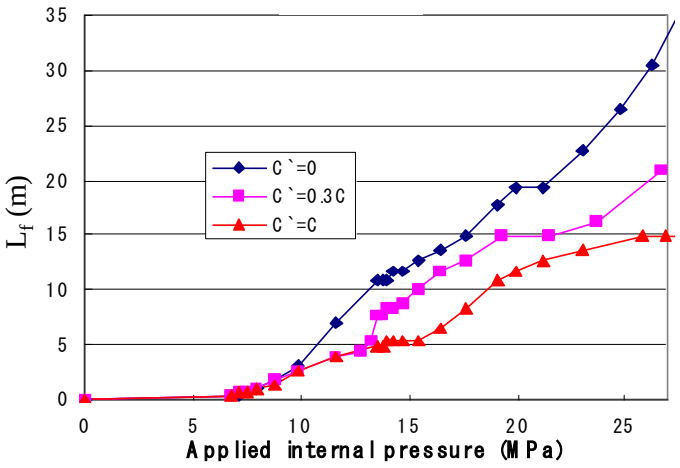

Figure 2.31 Failure lengths during applying internal pressure (Jongpradist et al., 2007)

It is seen that, for all cases, failure starts at the pressure of about 5 MPa and the failure length is longer with increasing internal pressure. The distinct difference among three cases can be seen after internal pressure applied is larger than 10 MPa. The third case, which assumes non-cohesion, yields the longest failure length at the same applied pressure. At the maximum operation pressure of 12 MPa, failure length of case 3 becomes about two times of others.

To evaluate the safety of cavern against internal pressure, an index which defines a ratio of non-failure path (1-Lf/L), is introduced and the analysis results can be illustrated as in Figure 2.32. The parameter L is the total predicted failure length.

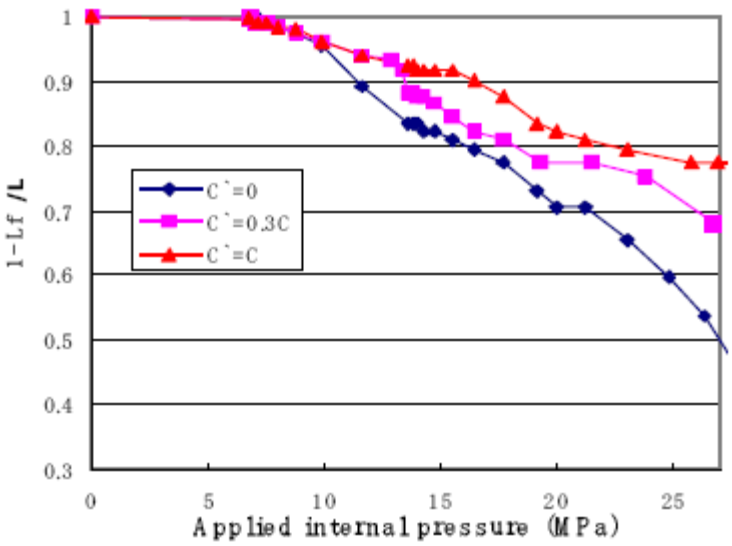

Figure 2.32 Ratio of non-failure path against internal pressure (Jongpradist et al., 2007)

The results indicate decrease in non-failure path ratio with increasing applied internal pressure with increasing trend. Only about a half of non-failure path remains at the pressure of 26 MPa if cohesion is not considered (case 3). The results of slip length at the important internal pressures are concluded in Table 2.4.The failure ratios for all cases are also included.

Table 2.4 Conclusion of analysis results (Jongpradist et al., 2007)

Case	Pressure (Mpa)	Strength parameters (rock mass/top soil)		Slip length Lf (m)	Failure ratio Lf/L (%)
		C (MPa)	(ϕ°)		
1	13.2	3.0/0.5	45/30	4.9	6.7
	15.6	3.0/0.5	45/30	6.5	9.0
	26.4	3.0/0.5	45/30	16.2	22.4
2	13.2	0.9/0.15	45/30	7.0	9.7
	15.6	0.9/0.15	45/30	8.8	12.2
	26.4	0.9/0.15	45/30	20.1	27.8
3	13.2	0.0	45/30	10.8	15.0
	15.6	0.0	45/30	13.6	18.8
	26.4	0.0	45/30	30.4	42.1